

PAPER • OPEN ACCESS

Two-color laser scattering for diagnostics of hydrogen plasma

To cite this article: Franciszek Sobczuk *et al* 2022 *Plasma Sources Sci. Technol.* **31** 115012

View the [article online](#) for updates and enhancements.

You may also like

- [Systematic experimental study on a highly efficient terahertz source based on two-color laser-induced air plasma](#)
Jun Xie, Wen-Hui Fan and Xu Chen
- [Scaling up and parametric characterization of two-color air plasma terahertz source](#)
S Saxena, S Bagchi, M Tayyab et al.
- [Investigation on a Novel Direct Liquid Fuel Cell Feeding on Oxaly Dihydrazide](#)
Tingjun Zhuang, Lei Yuan, Qiqi Wan et al.



HIDEN ANALYTICAL

Analysis Solutions for your Plasma Research

- Knowledge,
- Experience,
- Expertise

[Click to view our product catalogue](#)

Contact Hiden Analytical for further details:
W www.HidenAnalytical.com
E info@hiden.co.uk



Surface Science

- ▶ Surface Analysis
- ▶ SIMS
- ▶ 3D depth Profiling
- ▶ Nanometre depth resolution



Plasma Diagnostics

- ▶ Plasma characterisation
- ▶ Customised systems to suit plasma Configuration
- ▶ Mass and energy analysis of plasma ions
- ▶ Characterisation of neutrals and radicals

Two-color laser scattering for diagnostics of hydrogen plasma

Franciszek Sobczuk^{1,*}, Krzysztof Dzierżęga¹, Witold Zawadzki¹,
Bartłomiej Pokrzywka² and Evgeny Stambulchik³

¹ Marian Smoluchowski Institute of Physics, Jagiellonian University, ul. Łojasiewicza 11, 30-348 Kraków, Poland

² Institute of Physics, Pedagogical University, ul. Podchorążych 2, 30-084 Kraków, Poland

³ Faculty of Physics, Weizmann Institute of Science, Rehovot 7610001, Israel

E-mail: franciszek.sobczuk@doctoral.uj.edu.pl, krzysztof.dzierzega@uj.edu.pl,
witold.zawadzki@uj.edu.pl, bartlomiej.pokrzywka@up.krakow.pl and
evgeny.stambulchik@weizmann.ac.il

Received 13 August 2022, revised 26 September 2022

Accepted for publication 20 October 2022

Published 17 November 2022



Abstract

A two-color laser scattering (2CLS) method is proposed to measure electron and neutral densities, as well as electron and ion temperatures in hydrogen plasma. 2CLS uses two probe wavelengths to identify the Rayleigh scattering and Thomson scattering contributions coming from neutrals and electrons, respectively. Laser scattering signals were simulated for various conditions of a hydrogen plasma at thermodynamic equilibrium applying the available and calculated cross-sections for Rayleigh scattering by ground-state and excited hydrogen atoms at probe wavelengths of 355 nm and 532 nm. The developed 2CLS method was eventually applied to study the laser-induced plasma in hydrogen at near atmospheric pressure. Temporally and spatially resolved electron and ion temperatures and densities of electrons and hydrogen atoms (ground-state and excited) were determined.

Keywords: laser-induced plasma, Thomson scattering, Rayleigh scattering, two-colour Thomson scattering method, plasma diagnostics

(Some figures may appear in colour only in the online journal)


1. Introduction

Elastic scattering of laser light from bound and free electrons has become a standard method for plasma diagnostics [1, 2] providing temporally resolved information on local plasma parameters such as electron and neutral density, electron and ion temperatures, plasma flow/drift velocity, or electron energy distribution function. Laser scattering (LS) has been applied to investigate various types of glow-discharge plasmas [3–9],

pinch plasmas [10–13] and thermal plasmas such as welding arcs and plasma jets [14–24]. It has also played an important role in studies of fusion plasmas [25–28] where it is still the most reliable method for measuring electron temperature. Last but not least, it has been used to study laser-induced plasmas [29–36] of both low and high temperatures, the latter being related to inertial-confinement fusion research.

Apart from the high temporal and spatial resolution, LS allows direct measurements of plasma parameters without relying on local thermodynamic equilibrium (LTE) assumptions or non-LTE plasma models, as is the case with many commonly used methods of optical emission spectroscopy. LS has proven to be particularly useful in the diagnostics of hot gases and weakly ionized plasmas, as well as hot plasmas with LS spectra dominated by Rayleigh scattering (RS) and Thomson scattering (TS), respectively. However, in the case

* Author to whom any correspondence should be addressed.

 Original content from this work may be used under the terms of the [Creative Commons Attribution 4.0 licence](https://creativecommons.org/licenses/by/4.0/). Any further distribution of this work must maintain attribution to the author(s) and the title of the work, journal citation and DOI.

of a partially ionized plasma, both RS and TS can contribute significantly to LS, and their separation becomes indispensable for the reliable determination of electron and neutral densities.

In this work, we employ two probe lasers with very different wavelengths, such as the 2nd and 3rd harmonics of the Nd:YAG laser, to separate TS (electrons) and RS (neutral and molecular species) contributions and give separate estimates for the electron and neutral densities. This approach exploits different wavelength dependencies of the TS and RS cross sections and was originally proposed by Miles and Limbach [37] and is named two-color laser scattering (2CLS). This method resembles two-color interferometry [38–40] where the refractive index includes contributions from neutrals (which increases with wavelength) and electrons (which decreases with wavelength). However, unlike 2CLS, two-color interferometry lacks temporal and spatial resolution and does not yield information on particle temperatures.

Here, we applied the 2CLS method to investigate laser-induced plasma in hydrogen at near atmospheric pressure. In section 2, RS and TS are briefly overviewed, and the relative LS intensities, at two probing wavelengths, are theoretically studied at various plasma conditions generated by the NASA CEA equilibrium code [41] and using calculated and available cross sections for RS on hydrogen atoms in the ground and excited states. In section 3 we describe the experimental setup, while section 4 contains experimental results from the 2CLS method, which gives the electron density, the electron and ion temperature, and also the neutral hydrogen densities separately in the ground and excited states. Our studies are summarized and concluded in section 5.

2. Laser light scattering by the plasma

The laser light incident into the plasma can be scattered elastically (Rayleigh and Thomson) and/or inelastically (Raman), which is associated with dipole radiation by accelerating charged particles (Thomson scattering) or dipole radiation due to polarization of neutrals and ions (Rayleigh and Raman scattering).

2.1. Rayleigh scattering

In the Rayleigh scattering process, the power scattered by atoms or molecules within the frequency range $d\omega$ and into the solid angle $d\Omega$ is given by

$$\frac{dP_R(\omega)}{d\Omega} d\omega = \eta P_L L \Delta\Omega \sum_j n_j \bar{\sigma}_{\Omega,j} S_{R,j}(\mathbf{k}, \omega) d\omega. \quad (1)$$

Here, η is the optical and detector efficiency coefficient, P_L is the average power of the incident laser beam, L the length of the scattering volume, and $\Delta\Omega$ the detection solid angle. Furthermore, n_j is the number density of individual particles, while $\bar{\sigma}_{\Omega,j}$ is the mean differential cross-section defined as

$$\bar{\sigma}_{\Omega,j} = \sum_i q_{j,i} \frac{d\sigma_{j,i}}{d\Omega} \quad (2)$$

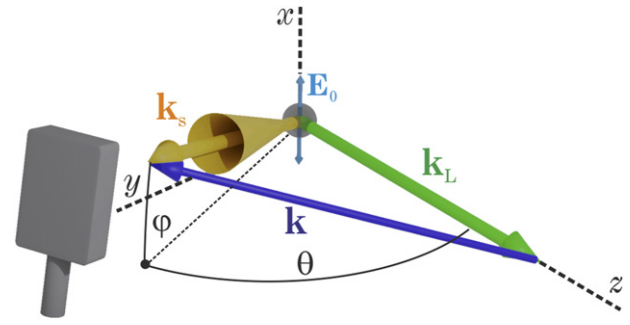


Figure 1. Typical geometric arrangement of the laser scattering experiment. \mathbf{E}_0 , \mathbf{k}_L and \mathbf{k}_s are the electric vector, the wavevector of the incident laser beam and the wavevector of scattered light, respectively. $|\mathbf{k}| \equiv |\mathbf{k}_s - \mathbf{k}_L| = (2\pi/\lambda_L)2 \sin(\theta/2)$ is the scattering wavevector, while θ and φ are the scattering angles.

where $q_{j,i}$ is the fraction of the j th species in its i th state while $d\sigma_{j,i}/d\Omega$ is the corresponding differential cross-section for RS. Finally, $S_{R,j}(\mathbf{k}, \omega)$ denotes the spectral density function of the Rayleigh–Brillouin feature [42]. This feature takes on different spectral shapes depending on the y parameter given by

$$y \equiv 1/(kd), \quad (3)$$

where $k = 2\pi/\lambda$ is the scattering wave vector with λ the scattering wavelength, while d is the mean free path of the particles. The scattering wavelength $\lambda = \lambda_L(2 \sin(\theta/2))$ is determined solely by the geometry of the experiment (see figure 1) where θ is the scattering angle defined relative to the laser propagation direction, while λ_L is the laser wavelength. For hot gases and plasmas under a typical experimental arrangement ($\theta = 90^\circ$, $\varphi = 0^\circ$, $\lambda_L = 532$ nm), henceforth referred to as standard configuration, $y \ll 1$ (Knudsen regime) and $S_{R,j}(\mathbf{k}, \omega)$ has a Gaussian shape reflecting the thermal motion of scattering particles.

The cross section for Rayleigh scattering of linearly polarized light by atoms in a given state was calculated by Penney [43]. The scattered light consists of that maintaining polarization (polarized) and a depolarized one, that is, for the scattering configuration considered here, polarized in the direction of the incident probe beam. For an atom in the initial state denoted by $|T, J, M\rangle$, where J is the total angular momentum quantum number, M is the magnetic quantum number and T represents all other quantum numbers (including the principal quantum number n), the differential cross-section for the polarized component and for incident light of wavelength $\lambda_0 = 2\pi c/\omega_0$ is [43]

$$\left(\frac{d\sigma}{d\Omega}\right)_{p(TJ)} = 9(2J+1)\omega_0^4 \left(\frac{e^2}{4\pi\epsilon_0 m_e c^2}\right)^2 \times \sum_M \left[\sum_{T', J'} \frac{f_{TJ, T'J'}}{\omega_{T'J', TJ}^2} \begin{pmatrix} J' & 1 & J \\ -M & 0 & M \end{pmatrix} \right]^2 \quad (4)$$

while for the depolarized component

$$\left(\frac{d\sigma}{d\Omega} \right)_{d(TJ)} = \frac{9}{4} (2J+1) \omega_0^4 \left(\frac{e^2}{4\pi\epsilon_0 m_e c^2} \right)^2 \sum_M \left\{ \sum_{T'J'} \frac{f_{TJ,T'J'}}{\omega_{T'J',TJ}} \right.$$

$$\times \left[\frac{\begin{pmatrix} J' & 1 & J \\ -M & 1 & M-1 \end{pmatrix} \begin{pmatrix} J' & 1 & J \\ -M & 0 & M \end{pmatrix}}{\omega_{T'J',TJ} - \omega_0} + \right.$$

$$\left. \left. - \frac{\begin{pmatrix} J' & 1 & J \\ 1-M & 0 & M-1 \end{pmatrix} \begin{pmatrix} J' & 1 & J \\ 1-M & -1 & M \end{pmatrix}}{\omega_{T'J',TJ} + \omega_0} \right]^2 \right\} \quad (5)$$

In these equations, T' and J' are quantum numbers of virtual intermediate states, $\omega_{T'J',TJ}$ is the frequency of the $|TJ\rangle \rightarrow |T'J'\rangle$ transition, $f_{TJ,T'J'}$ denotes the oscillator line strength for the transition while e , m_e and c are the electron charge and mass and the speed of light in a vacuum, respectively. These formulas are valid if

$$|\omega_0 - \omega_{T'J',TJ}| \gg \gamma_{T'J',TJ} \quad (6)$$

for all transitions $|TJ\rangle \rightarrow |T'J'\rangle$, where $\gamma_{T'J',TJ}$ is the width of the transition line. Otherwise, resonance effects must also be taken into account.

Figure 2 shows the total differential cross-section and its depolarized component for RS on the hydrogen atom in both the ground and excited states with a principal quantum number of up to $n = 7$ calculated using equations (4) and (5). These cross-sections were derived for scattering at wavelengths of the second (532 nm) and third (355 nm) harmonics of the Nd:YAG laser and for the standard experimental configuration. The corresponding oscillator line strengths were calculated according to the formulas presented by Sobelman [47] while the summation of the series in equations (4) and (5) was performed including all virtual states $|T'J'M'\rangle$ up to $n = 50$. It was verified that there were no significant contributions originating from higher virtual states.

The cross-sections for a given state $|n\rangle$ shown here are average values determined on the basis of the cross sections for states with all possible angular momentum values weighted by their degeneracy. The results of these calculations indicate that the cross-sections for the RS by the ground-state atoms are more than two orders of magnitude smaller than those by the excited atoms. Moreover, the cross section for the polarized RS is significantly larger than for the depolarized one, and, importantly, it becomes wavelength independent with increasing n . The only exception is the state $n = 3$ for which both types of scattering, at 532 nm wavelength, are of equal probability, which is likely due to its near-resonance character. As can be seen in figure 2, the cross-sections for RS in hydrogen calculated in this work are about 50% smaller than those presented in the works of Gavrilu [44, 45] and

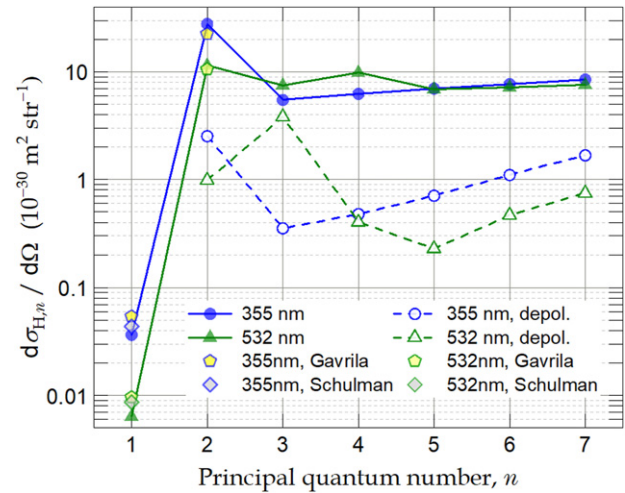


Figure 2. Total differential cross sections and their depolarized component for RS by hydrogen atom at wavelengths of 355 nm and 532 nm. The total cross sections obtained by Gavrilu [44, 45] and Schulman [46] are shown for comparison.

Schulman [46]. This discrepancy could originate from the simplification of the Rayleigh scattering model used in the present work. This model (equations (4) and (5)) contains only summation over discrete atomic states. Calculations based on extended model, containing also integration over continuum states, as described in [48], will be presented in the future work.

To assess the magnitude of the RS signal in a hydrogen plasma, its composition was first determined in dependence on pressure and temperature. Calculations were performed using the NASA CEA equilibrium code [41] assuming that the plasma is in local thermodynamic equilibrium, and the results are presented in figures 3(a)–(d). As one can observe, at about 5000 K hydrogen is largely dissociated, and the number of atoms is the highest. A further increase in temperature results in a reduction in the number of atoms and a rapid increase in the number of electrons and protons.

Figures 3(e)–(l) show the temperature dependence of the total RS signal (polarized and depolarized) and its different contributions calculated for the second and third harmonic of the Nd:YAG laser and for the standard experimental configuration. These signals are normalized to the reference signal originating from a molecular hydrogen gas under ambient conditions, that is, at a pressure of 1 bar and at 295 K room temperature and are defined as

$$r_j = \left(\frac{dP_j}{d\Omega} \right) \left(\frac{dP_{\text{ref}}}{d\Omega} \right)^{-1}$$

$$= \left(\frac{n_j}{n_{\text{ref}}} \right) \left(\frac{d\sigma_{\text{ref}}}{d\Omega} \right)^{-1} \sum_i q_{j,i} \frac{d\sigma_{j,i}}{d\Omega} \quad (7)$$

where $n_{\text{ref}} = n_{\text{H}_2} = 2.463 \times 10^{25} \text{ m}^{-3}$ while $d\sigma_{\text{ref}}/d\Omega$ is 7.21×10^{-32} and $1.333 \times 10^{-32} \text{ m}^2 \text{ sr}^{-1}$ at 355 nm and 532 nm, respectively [49].

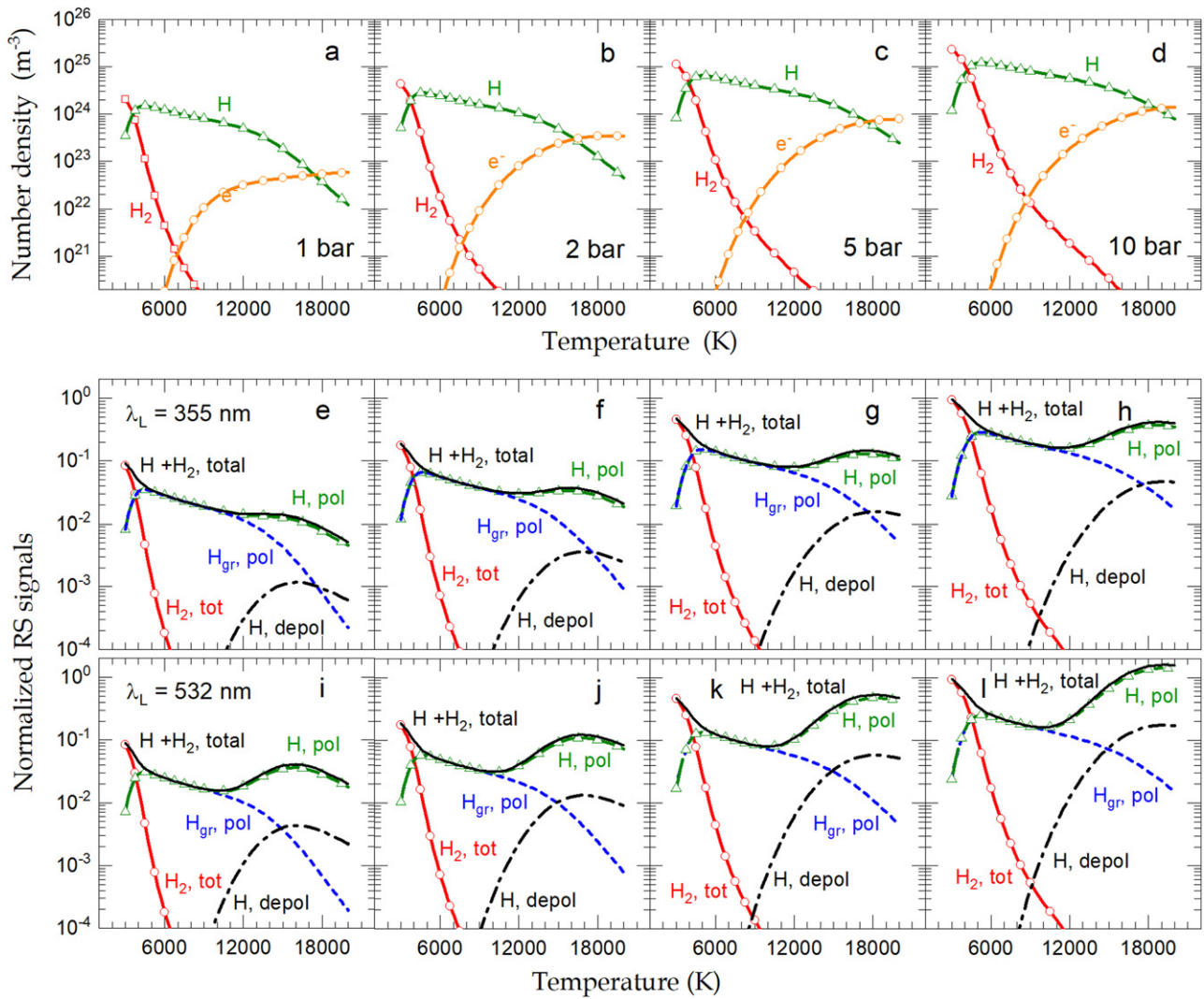


Figure 3. (a)–(d) Hydrogen plasma composition calculated using NASA CEA equilibrium code [41]. (e)–(l) Various contributions to the RS signals calculated at wavelengths of 355 nm and 532 nm and normalized to the reference RS signal from H_2 molecular gas at a pressure of 1 bar and at room temperature of 295 K. All calculations made for a typical experimental configuration, i.e. $\theta = 90^\circ, \varphi = 0^\circ$ and for the plasma composition shown in figures (a)–(d).

In the studied range of plasma temperature, for both probe wavelengths, the total RS signal initially decreases with temperature, then rapidly increases, reaching its maximum value, and then starts to decrease again. However, except for the case of the highest pressure investigated for the wavelength of 532 nm and simultaneously for a high plasma temperature (see figure 3), this signal is always lower than the reference one. Despite the large RS cross sections for scattering by excited atoms, the polarized signal, due to ground-state atoms, is dominant up to about 1000 K, while that due to excited-state atoms prevails above 12000 K. However, the significance of the depolarized signal increases with temperature but still remains at least an order of magnitude smaller than the polarized one.

2.2. Thomson scattering

Thomson scattering is mainly due to non-relativistic electrons, as their mass is much lower than the mass of ions, resulting

in a much higher acceleration in the electric field of the laser beam and, consequently, in much stronger dipole radiation. TS measures fluctuations in electron density co-propagation and counter-propagation along the scattering wave vector \mathbf{k} (see figure 1). Similarly to RS, the scattered power around the scattering angle θ and within the frequency range $d\omega$ as a function of the frequency shift $\omega = \omega_s - \omega_L$ is given by

$$\frac{dP_T(\omega)}{d\Omega} d\omega = \eta P_L L \Delta\Omega n_e \frac{d\sigma_T}{d\Omega} S_T(\mathbf{k}, \omega) d\omega \quad (8)$$

where n_e is the electron density while $d\sigma_T/d\Omega = r_e^2(1 - \sin^2\varphi \cos^2\theta)$ is the differential cross-section for the TS of an electromagnetic wave by a free electron with r_e the classical electron radius.

The spectral density function $S_T(\mathbf{k}, \omega)$ depends on the scattering geometry, the laser wavelength, and plasma properties, and its spectrum results from the motion of the electrons and their correlation. For plasmas with a Maxwellian velocity distribution but with different electron and ion temperatures,

after Salpeter approximation, the spectral density function is [50, 51]

$$\begin{aligned}
 S_T(\mathbf{k}, \omega) d\omega &= S_e(\mathbf{k}, \omega) d\omega + S_i(\mathbf{k}, \omega) d\omega \\
 &= \left| \frac{1 + \alpha^2 Z(T_e/T_i)W(x_i)}{1 + \alpha^2 W(x_e) + \alpha^2 Z(T_e/T_i)W(x_i)} \right|^2 \\
 &\quad \times \frac{\exp(-x_e^2)}{\pi^{1/2}} dx_e \\
 &\quad + Z \left| \frac{-\alpha^2 W(x_e)}{1 + \alpha^2 W(x_e) + \alpha^2 Z(T_e/T_i)W(x_i)} \right|^2 \\
 &\quad \times \frac{\exp(-x_i^2)}{\pi^{1/2}} dx_i. \tag{9}
 \end{aligned}$$

Here, $x_e = \omega/(kv_e)$ and $x_i = \omega/(kv_i)$ where $v_{ei} = \sqrt{(2k_B T_{e,i}/m_{e,i})}$ is the thermal mean velocity of electrons (e) or ions (i), Z is the charge number of the ion, while $W(x)$ is the plasma dispersion function. The scattering parameter

$$\alpha \equiv 1/(k\lambda_D) \tag{10}$$

where $\lambda_D = (\epsilon_0 k_B T_e/n_e e^2)^{1/2}$ is the electron Debye length, ϵ_0 is the permittivity of the free space, and k_B Boltzmann's constant.

Two terms in equation (9), after Salpeter, are named the electron and ion features, and their spectra take on different shapes depending on the scattering parameter α . For $\alpha \ll 1$, properties of the electron feature are determined by the motion of individual uncorrelated electrons, which is termed non-collective scattering, and then the resulting spectrum reflects the electron energy distribution. For the Maxwellian distribution, the electron temperature T_e can be derived from the half-width of the scattering spectrum, while n_e is determined by calibrating the total scattered power using Rayleigh or Raman scattering spectra recorded for some reference gas [52]. With increasing α , the collective motion of electrons prevails and completely determines the electron part of the TS spectrum for $\alpha \gg 1$. This type of TS is called collective and is characterized by two satellites in the scattered spectrum at a distance $\Delta\omega = \omega - \omega_L = \pm(\omega_{pe}^2 + 3k_B T_e k^2/m_e)^{1/2}$ from the laser frequency with $\omega_{pe} = (n_e e^2/m_e \epsilon_0)^{1/2}$ the electron plasma frequency. In the case of collective and partially collective ($\alpha \cong 1$) scattering, the fundamental plasma parameters, n_e and T_e , are unambiguously determined by fitting the spectral density function to the electron part of the experimental TS spectra without the need to calibrate their power [53].

On the other hand, the ion component, in addition to n_e and T_e is also dependent on T_i , which can be used, for example, to measure the temperature of ions (heavy particles) in two-temperature non-isothermal plasmas.

The spectra of the spectral density function, of its electron and ion contribution, for different α , are shown in figures 4(a)–(d).

In addition to the fact that α determines the TS spectrum, it has a significant impact on the total intensity of the scattered light, since the spectrally integrated spectral density function

is α dependent

$$\begin{aligned}
 S_T(\mathbf{k}) &\equiv \int S_T(\mathbf{k}, \omega) d\omega = S_e(\mathbf{k}) + S_i(\mathbf{k}) \\
 &= \frac{1}{1 + \alpha^2} + \frac{Z\alpha^4}{(1 + \alpha^2)(1 + \alpha^2(1 + ZT_e/T_i))}. \tag{11}
 \end{aligned}$$

As is clear from equation (11), although S_T decreases with α , the contribution of the ionic part increases, depending on the ratio of the electron temperature to the ion temperature. The amplitude of S_T varies particularly strongly with the ratio T_e/T_i for $\alpha \gtrsim 1$.

The ion component occurring in the central part of the TS spectrum (at the wavelength of the probe laser) is spectrally two orders of magnitude narrower than the electron component (see figures 4(a)–(d)). Therefore, in principle, these components are easily distinguishable and separable. However, the very small spectral bandwidth of this component and its overlap with the RS signal, which inherently accompanies TS in low-temperature plasmas, are the main experimental challenges.

Figures 5(a)–(d) show the temperature dependence of the scattering parameter α calculated for the hydrogen plasma conditions obtained using the NASA CEA code and for the standard experimental configuration considered in this work. As can be seen, initially α increases rapidly as a result of the fast growth of the electron number density. At a given pressure, a further increase in plasma temperature no longer results in a noticeable increase in n_e , so a slow drop in α is observed. On the other hand, for a given temperature, α increases with pressure and its maximum shifts toward higher temperatures from 2.83 at 16 500 K to 7.3 at 20 000 K for the pressure range studied and for the scattered wavelength of 532 nm. In the same way, α varies for the scattered wavelength of 355 nm except that it is a factor of 1.5 lower than for the probe wavelength of 532 nm.

The change in α along with the plasma temperature causes the change of the nature of TS, and hence its spectrum, from completely non-collective to collective or partially collective.

Figures 5(e)–(l) show the polarized component of the normalized total, RS, and TS light intensity as a function of plasma temperature. The RS dominates for low plasma temperatures, whereas at higher temperatures the total signal is dominated by the TS. In the latter range, the total intensity of scattered light can greatly exceed the reference one.

In general, the TS signal grows with temperature and pressure, but the growth rate of the ion contribution is much higher than that of the electron contribution for ever higher pressures. In particular, for the 532 nm wavelength (larger scattering parameter α) and for a correspondingly high temperature, the ion contribution becomes greater than the electron contribution. Although the intensity of the electron feature is high, say at 14 000 K, its large spectral width means that only its small fraction falls into the spectral band of the ion feature, which is about 20–50 pm in typical experiments in

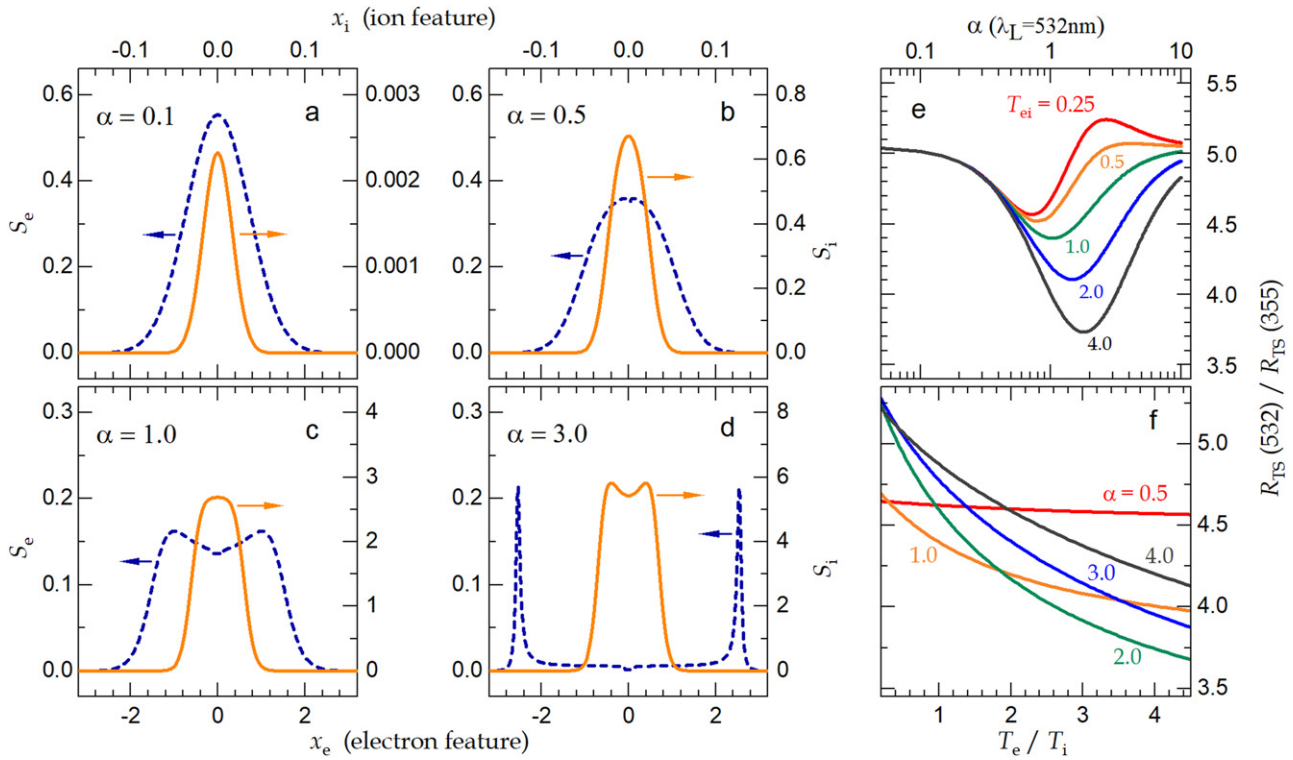


Figure 4. The spectral density function (defined by equation (9)) of the electron (dashed blue line) and the ion features (full orange line) for different scattering parameters α and for isothermal ($T_e = T_i$) plasma conditions (a)–(d). The ratio $R_{TS}(532)/R_{TS}(355)$ of the normalized total intensities of TS signals at probe wavelengths of 532 nm and 355 nm for given T_e/T_i depending on α at 532 nm (e) and for given α depending on T_e/T_i (f).

a low-temperature plasma. In contrast, the spectral width of the ion feature is similar to the bandwidth of the detection optics and therefore perfectly matches the RS signal, which increases significantly at higher temperatures because of scattering on larger and larger number of excited-state hydrogen atoms.

2.3. Two-color laser scattering (2CLS)

It is clear from the above considerations that it is impossible to assess, on the basis of measurements for a single wavelength, whether Rayleigh or Thomson scattering is responsible for the observed radiation scattered by the plasma. Moreover, it is not clear whether Rayleigh scattering is caused by ground-state or excited hydrogen atoms, or whether Thomson scattering is due to the ion or electron feature. In the latter case, it is certainly helpful to measure the spectrum of the scattered light because of the significant difference in the spectral widths of these two features. Unfortunately, the separation of the remaining contributions, i.e. the ion part of TS and RS, is impossible under experimental conditions with a typical spectral resolving power. However, by taking advantage of the different wavelength dependencies of RS and TS, this ambiguity can be resolved using two different wavelengths. This approach, two-color light scattering (2CLS), involves application of two probe laser beams of significantly different wavelengths, e.g., the second and third harmonics of a Nd:YAG laser.

The total intensity of the scattered light, normalized to the reference signal, for a given laser wavelength λ_k is

$$R_k = \frac{I_{LS}(\lambda_k)}{I_{LS}^{ref}(\lambda_k)} = \left[n_{Hgr} \frac{d\sigma_{gr}}{d\Omega} + n_H^* \frac{d\sigma_H^*}{d\Omega} + n_e \frac{d\sigma_T}{d\Omega} \right] \left(S_e(n_e, T_e) + S_i(n_e, T_e, T_i) \right) \left(n_{ref} \frac{d\sigma_{ref}}{d\Omega} \right)^{-1} \quad (12)$$

where n_{Hgr} , n_H^* and n_e are the number densities of the ground-state and excited hydrogen atoms and electrons, respectively. Each of the four contributions depends on the wavelength of the probe laser beam differently. However, the first is wavelength independent, because both $d\sigma_{gr}/d\Omega$ and $d\sigma_{ref}/d\Omega$ scale as $1/\lambda_k^4$. In equation (12) we introduce two RS contributions, from hydrogen atoms in their ground and excited states. Such a division results from the substantially different wavelength dependencies of the respective Rayleigh scattering cross sections. Furthermore, except for LTE plasma, there is no simple relation between n_{Hgr} and n_H^* . Here, $d\sigma_H^*/d\Omega$ represents the effective differential cross-section for RS by excited hydrogen atoms, which we define as

$$\frac{d\sigma_H^*}{d\Omega} = \sum_{n=2} \sum_J \frac{(2J+1)}{Z(T)} \exp\left(-\frac{E(n, J)}{k_B T}\right) \frac{d\sigma_H(n, J)}{d\Omega}. \quad (13)$$

$d\sigma_H(n, J)/d\Omega$ and $E(n, J)$ are the differential RS cross section and energy of the state $|n, J\rangle$, respectively, and $Z(T)$ is the temperature-dependent partition function for the ensemble of excited hydrogen atoms. Thus, the contribution of the state

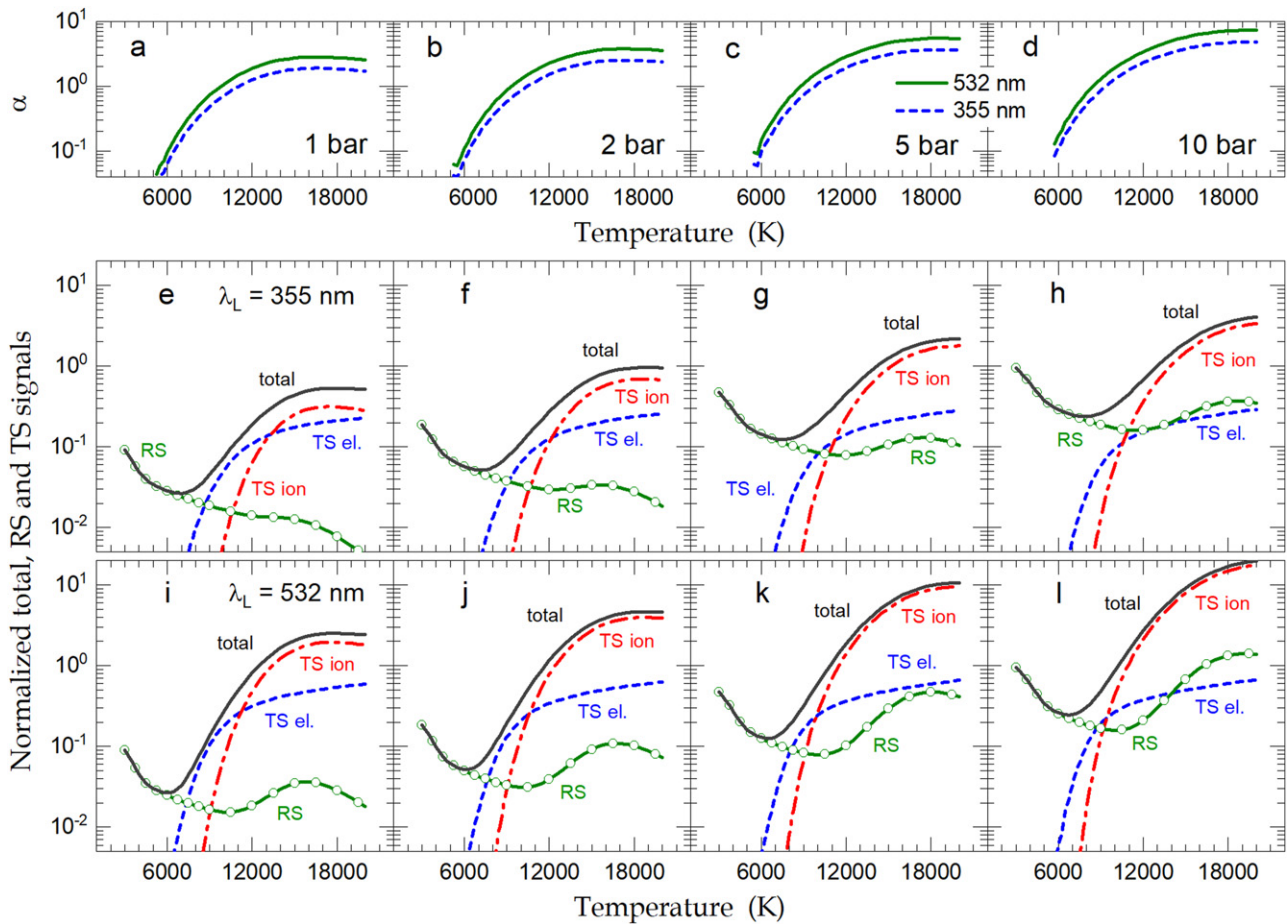


Figure 5. The TS scattering parameter for hydrogen plasma composition calculated using NASA CEA equilibrium code (a)–(d). Various contributions to the scattered signal calculated at wavelengths of 355 nm and 532 nm and normalized to the reference RS signal from H₂ molecular gas at a pressure of 1 bar and at room temperature of 295 K (e)–(l). All calculations are made for a typical experimental configuration, i.e. $\theta = 90^\circ$, $\varphi = 0^\circ$ and for the plasma composition shown in figures 3(a)–(d).

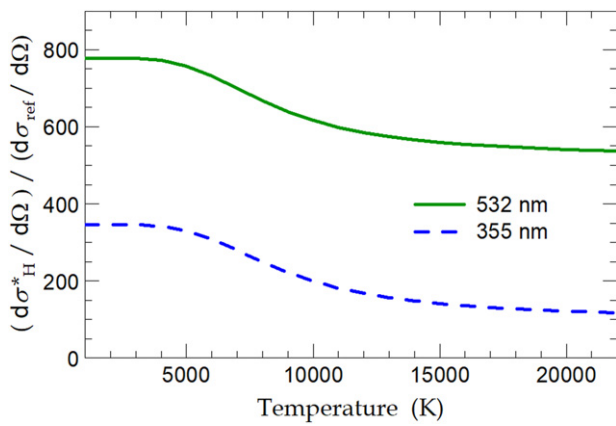


Figure 6. Temperature dependence of the normalized effective differential cross-sections for polarized Rayleigh scattering at wavelengths of 355 nm and 532 nm, for hydrogen atoms in the excited states.

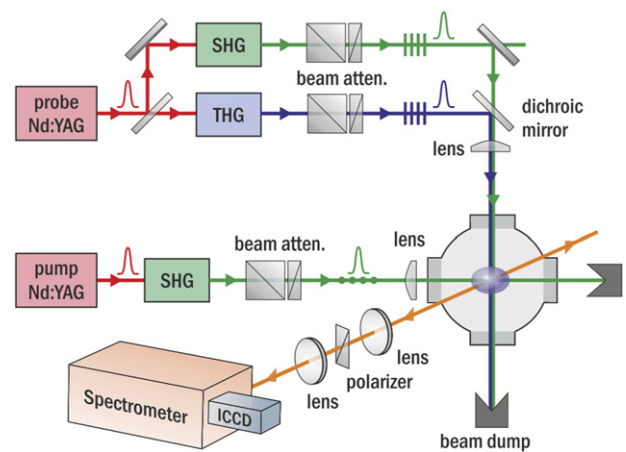


Figure 7. Experimental setup.

$|n, J\rangle$ to the effective cross-section is weighted by its relative population. The latter, assuming plasma at least in the partial LTE, is governed by the Boltzmann factor and the degeneracy of the state. Figure 6 shows the normalized $d\sigma_{\text{H}}^*/d\Omega$ versus

plasma temperature for polarized Rayleigh scattering at wavelengths of 355 nm and 532 nm. Both quantities decrease with temperature, especially in the range of 5000 K to 12000 K, with the scattering at 355 nm being more sensitive. This

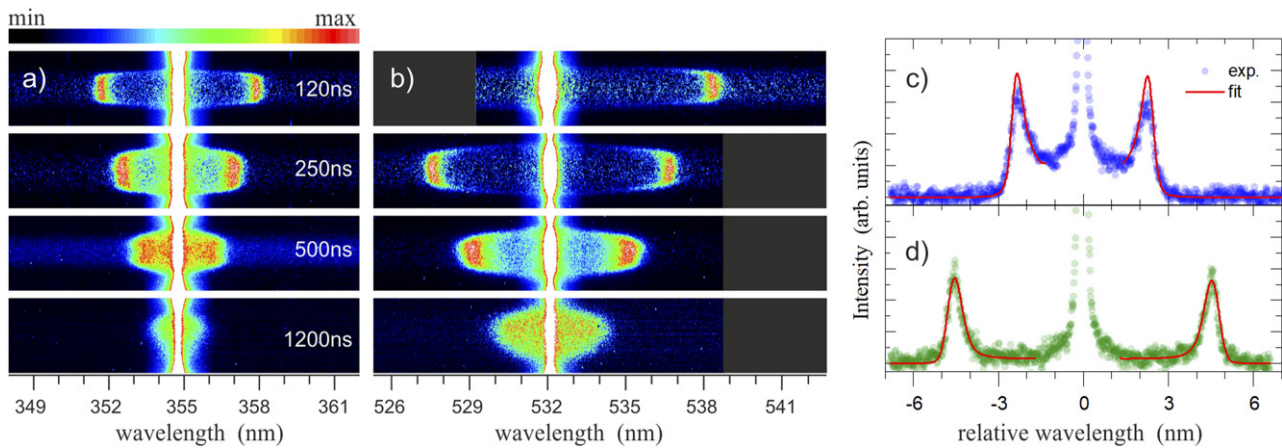


Figure 8. (a) and (b). Images of LS spectra obtained with probe lasers of 355 nm (a) and 532 nm (b) for different delays. (c) and (d). Measured and fitted TS spectra for a delay of 250 ns on the plasma axis for two probe lasers of 355 nm (c) and 532 nm (d). The mean electron number density and electron temperature are $2.09(31) \times 10^{23} \text{ m}^{-3}$ and 14 470(705) K, respectively. Standard deviation of the electron density distribution is equal to 15.3%.

behavior can be explained by lowering the relative contribution of the state with $n = 2$, which is characterized by the largest cross-sections (see figure 2).

The sensitivity of the 2CLS method to ionic temperature is shown in figures 4(e) and (f). It is evident that the ratio of the normalized total TS signals at the probe wavelengths considered undergoes particularly strong variations for α in the range from about 1 to about 5–6.

Equation (12) contains 5 unknowns (n_{H}^{gr} , n_{H}^* , n_{e} , T_{e} , and T_{i}) and is an underdetermined system. The number of unknowns can be reduced by inferring n_{e} and T_{e} from the electron part of the TS spectrum and acquiring a pair $\{R_{355}, R_{532}\}$. In this way, there are now 2 equations and 3 unknowns that can be unambiguously computed, but with additional premises about the plasma state.

3. Experiment

The 2CLS method has been applied to investigate the laser-induced plasma in hydrogen, and a simplified scheme of the experimental setup is presented in figure 7. A vacuum chamber was evacuated below $[10^{-5}]$ mbar and then filled with pure hydrogen at 1300 mbar. Plasma was created in the center of the chamber by focusing a second-harmonic ($\lambda = 532 \text{ nm}$) Q-switched Nd:YAG laser pulse (4.5 ns duration, 10 Hz repetition rate and 115 mJ) with a 50 mm focal length aspheric lens. A laser spot of about $46 \mu\text{m}$ in diameter resulted in a laser fluence of about 2.4 kJ cm^{-2} .

For laser scattering experiments, another (single-mode, $\delta\lambda < 0.5 \text{ pm}$, 6 ns duration, 10 Hz repetition rate) Nd:YAG laser was used together with the second and third harmonic generators. The resulting pulses of wavelengths 532 nm and 355 nm were attenuated to energies of 1 mJ and 2 mJ, respectively, using Rochon prism polarizers and appropriate half-wave plates and then combined with a dichroic mirror. These probe laser beams, focused to spots of about $60 \mu\text{m}$ in diameter in the plasma volume, propagated orthogonally

to the pump, the plasma-generating one, and were polarized perpendicularly to the direction of observation. The delay between pump and probe pulses was controlled by a digital delay pulse generator with an accuracy better than 200 ps.

Plasma and laser scattered light were observed perpendicularly to laser beams by imaging the investigated area of plasma onto the entrance slit of a Czerny–Turner spectrometer (750 mm focal length, 0.502 nm mm^{-1} maximal reciprocal dispersion) with a magnification factor of 1.2. A polarizer was inserted into the path of the measured light to remove the depolarized part of the scattered light.

Plasma imaging was accomplished in the zeroth order of the spectrometer with a fully open entrance slit. Such imaging allowed for the verification of plasma reproducibility and the selection of the appropriate layer for further investigation. Laser-scattered light was recorded at probe laser wavelengths in the range that covers 6.65 nm and with an entrance slit of the spectrometer of $50 \mu\text{m}$.

Optical signals were recorded with a gated two-dimensional intensified charge-coupled device (ICCD) camera mounted in the focal plane of the spectrometer. The ICCD was synchronized to probe pulses. To improve the signal-to-noise ratio of the LS spectra, the ICCD gate width was as short as 8 ns. The spectra were averaged over 30 000–60 000 laser shots and studied in the time interval (time delay) from 120 ns to 1200 ns after the pump pulse. A very large number of averages were due to the very low energy of probe pulses to avoid potential plasma heating in the inverse bremsstrahlung process. The spectral sensitivity of the experimental optical and detection systems was determined pixel by pixel using a calibrated halogen lamp.

4. Results and discussion

Images of the LS spectra, measured for different delays and with probe lasers of 355 nm and 532 nm, are shown in

Table 1. Parameters of 2CTS configuration and physical constants applied and used in our experiment and calculations.

Probe laser wavelengths	355 nm and 532 nm
Scattering angles, θ, φ	90 deg, 0 deg
Differential TS cross-section, $d\sigma_T/d\Omega$	$7.941 \times 10^{-30} \text{ m}^2/\text{sr}$
Differential RS cross-section on Ar [54]	
$d\sigma_{\text{Ar}}/d\Omega(355 \text{ nm})$	$2.862(43) \times 10^{-31} \text{ m}^2/\text{sr}$
$d\sigma_{\text{Ar}}/d\Omega(532 \text{ nm})$	$5.455(72) \times 10^{-32} \text{ m}^2/\text{sr}$
Differential RS cross-section on H_2^a ,	
$d\sigma_{\text{H}_2}/d\Omega(355 \text{ nm})$	$7.21(11) \times 10^{-32} \text{ m}^2/\text{sr}$
$d\sigma_{\text{H}_2}/d\Omega(532 \text{ nm})$	$1.333(17) \times 10^{-32} \text{ m}^2/\text{sr}$
Number density of H_2 molecules	
At reference conditions, N_{H_2}	$2.463 \times 10^{25} \text{ m}^{-3}$

^aValues determined in this work by measuring and comparing the respective Rayleigh scattering signals for hydrogen and argon.

figures 8(a) and (b). They have already been corrected for the plasma emission background, the laser stray light, the dark current of the CCD matrix, and the spectral sensitivity of the experimental system.

These spectra are composed of two distinct sidebands, corresponding to the electron feature of Thomson scattering and a much stronger central part, at the wavelengths of the probe lasers. The latter includes both the ionic feature of TS and RS by ground- and excited-state hydrogen atoms. In the case of a delay of 120 ns and probe laser of 532 nm only one side of the TS electron feature was possible to measure. Plasma parameters, n_e and T_e , were determined by fitting the normalized spectral density functions, convolved with the instrumental profile, to the electron part of the normalized experimental TS spectra. In the case of the plasma studied, the complete analysis takes into account the distribution of n_e resulting from some plasma inhomogeneity, its evolution during the collection time of LS signal on the CCD, and its shot-to-shot variability. These effects were included in the fitted functions assuming that n_e is subject to a normal distribution. At the same time, variations of T_e are neglected, assuming their minor impact on TS signals compared to n_e . All physical constants and experimental parameters used in our calculations are collected in table 1. In this work, the required differential cross-sections for Rayleigh scattering by the reference H_2 gas were determined against the respective differential cross sections for argon given by Thalman *et al* [54]. For this purpose, the respective Rayleigh scattering measurements were performed. The results of the fit to the normalized TS spectra, recorded for the plasma on-axis and for the delay of 250 ns, are presented in figures 8(c) and (d).

Figure 9 shows the radial distribution of the mean electron number density and electron temperature for different delays that were determined from the electron parts of the normalized TS spectra. It is evident that n_e drops much faster than T_e , that is, from about $4.3 \times 10^{23} \text{ m}^{-3}$ to $1.2 \times 10^{22} \text{ m}^{-3}$ in the plasma core, in the delay range studied, while the temperature drops only by 60%, that is, from about 21 800 K to 8600 K. Moreover, both parameters are very homogeneous

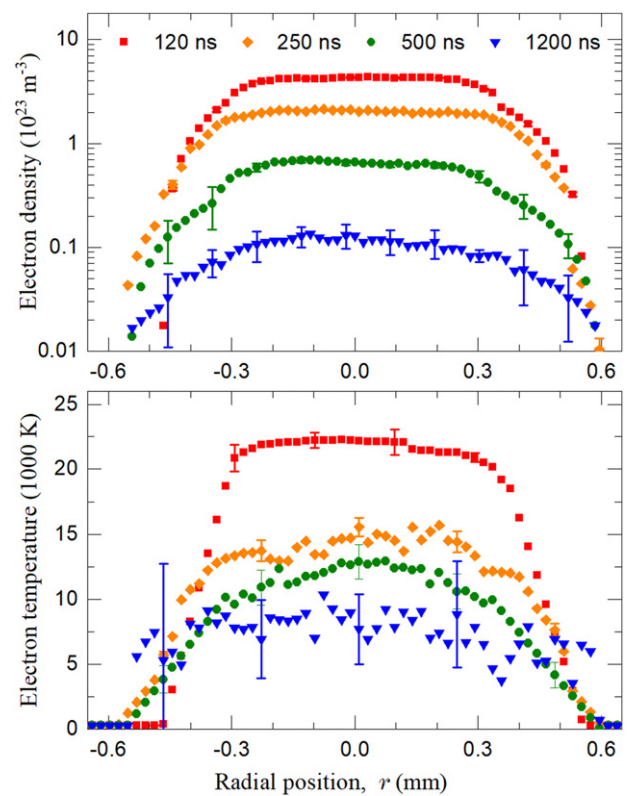


Figure 9. Radial distributions of the mean electron number density and electron temperature that were determined from the electron feature of TS spectra while assuming n_e to be subject to normal distribution.

in the plasma core, indicating that, at least for this plasma region, the measured distribution of n_e at the beginning of plasma evolution should be attributed to its variations during the measured interval and to limited plasma reproducibility, while at much longer delays only the latter comes into play.

As already mentioned, to determine other plasma parameters, such as the number density of hydrogen atoms in the ground and excited states and the ionic temperature, it is

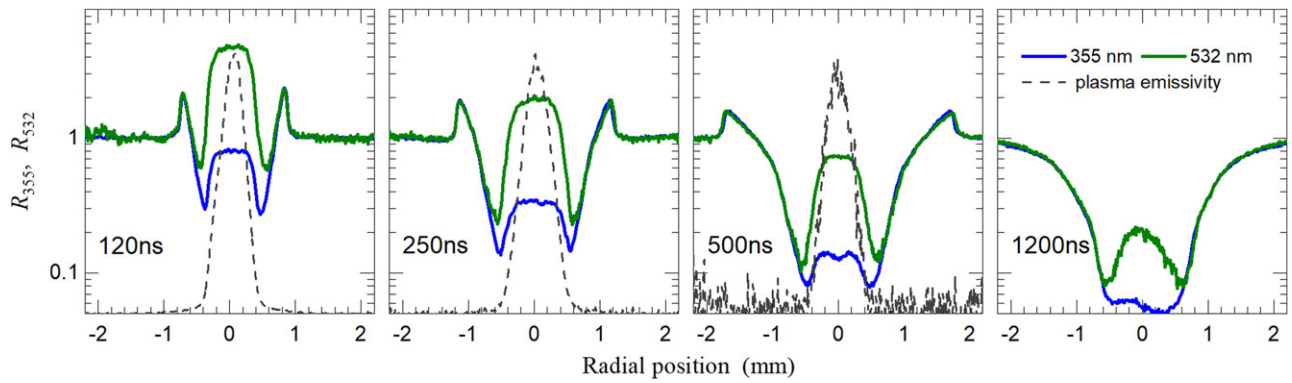


Figure 10. Measured radial distributions of the total scattering signals with probe lasers of 355 nm and 532 nm and the plasma emissivity recorded at 532 nm. The LS signals are normalized to the respective RS signals from the reference H_2 gas at 1300 mbar. The emissivity data are in linear scale.

necessary to make some assumptions about the plasma under study. These premises can be inferred, for example, by analyzing the radial distributions of the total, spectrally integrated and normalized intensities R_k of the polarized LS, which are shown in figure 10. In these figures, along with scattered light, the plasma emissivity is also shown. In the case of a delay of 1200 ns, light from the plasma was already too low to be observed during the 8 ns collection time on the ICCD camera.

At large radius, outside the plasma plume, R_{355} and R_{532} are identical and equal to unity, because they originate exclusively from scattering by the ambient H_2 gas. As the plasma is approached, except for 1200 ns, a sudden increase in the scattering signals is observed. Then both begin to decline; the slower the longer the delay, until the minima are reached. This region corresponds to the propagating shock wave, and as long as these scattering signals are identical, the scattering occurs predominantly on hydrogen molecules and ground-state atoms. The decrease in R_k intensity is due to reduced pressure, that is, a lower particle density behind the shockwave. The observed minima are preceded by the separation of the scattering signals with R_{532} exceeding R_{355} . Such separation implies the participation of scattering processes with probe wavelength dependencies different from those processes dominating the reference signals. Therefore, it can be assumed that in this plasma region the degrees of dissociation and ionization are increased, i.e. the number of electrons is increasing, which is also evidenced by the gradual increase of the plasma emissivity. Moreover, there are also spectral lines that indicate an increase in the number density of hydrogen atoms in their excited states. In the plasma core ($|r| < 0.2$ mm), the two signals are largely separated, which implies the dominance of LS on electrons and excited state atoms. Importantly, R_{532} is always significantly higher than R_{355} , which is in line with our calculations (see figure 5).

Based on these observations and calculations made, we can conclude that in the vast part of our plasma, where the electron temperature exceeds roughly 11 000 K, the main contribution to the LS signals comes from electrons and excited hydrogen atoms, but the electron contribution is highly dominant. In other plasma regions, the contribution to the

scattering signals, apart from electrons, comes from ground-state hydrogen atoms, and they play an increasingly dominant role as the temperature drops, i.e. at the edges of the plasma.

The ion temperature and the hydrogen atom density were eventually determined using the system of 2 equations (equation (12)) for the LS signal for two probe lasers, but also employing the predetermined electron number density and electron temperature. Two cases were considered. The first is that we deal with a two-temperature ($T_i \neq T_e$) plasma and that the population of all hydrogen levels is governed by the Boltzmann distribution with an excitation temperature equal to T_e . In this way, T_i and the total population of hydrogen atoms ($n_{H_{tot}}$) were unambiguously determined and the results are presented in figures 11 and 12, respectively. It is found that in the core of the plasma at the shortest delay, T_i is considerably higher than T_e , whereas in other cases they are comparable within uncertainty limits. Plasmas with $T_i > T_e$ are not unusual and in fact are encountered in laboratory experiments [55] as well as in space and Earth, as is the case with supernova remnants [56, 57] and Earth's plasma sheet [58]. Here, ion temperature in excess of electron temperature can be explained by the rapid cooling of the electrons in the radiative emission process, much faster than their energy exchange with heavy particles. Unfortunately, no T_i was evaluated for the longest delay due to the very poor contribution of the ionic feature to the total TS signal for the probe wavelength of 355 nm. On the other hand, the density of hydrogen atoms $n_{H_{tot}}$ is always the lowest in the center of the plasma and increases with delay. For delay of 1200 ns it is about $2 \times 10^{24} \text{ m}^{-3}$. In the other three cases, it is below the detection limit, which we estimate to be about $2.5 \times 10^{23} \text{ m}^{-3}$. As expected, in all cases there is an increase in $n_{H_{tot}}$ in the periphery and beyond plasma limits.

In the second approach, we assume that $T_i = T_e$, and that the populations of ground-state and excited hydrogen atoms are not related by the Boltzmann distribution. In this way, we independently obtain the densities of these two types of particles. As can be seen in figure 12, the maxima of n_{H^*} correspond to the minima of $n_{H_{gr}}$. Moreover, the population of the excited atoms decreases with time from about

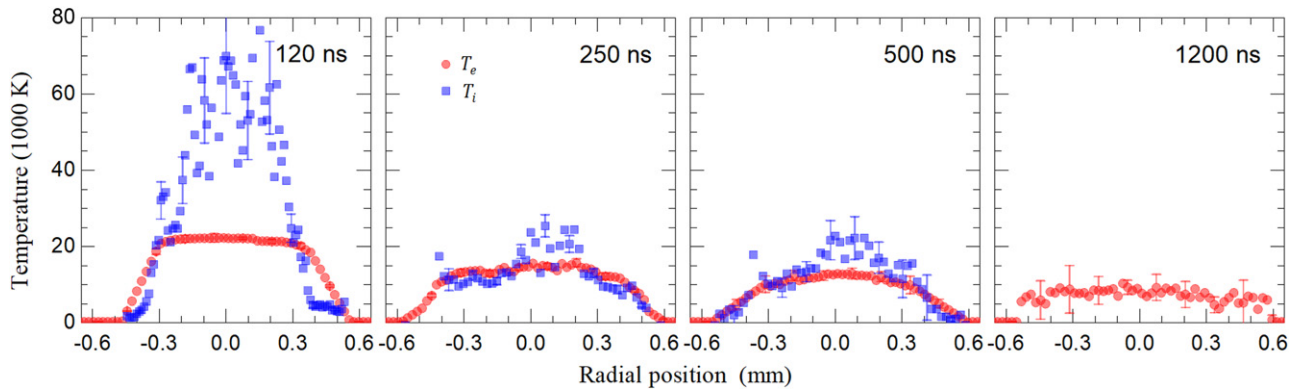


Figure 11. Radial distributions of electron (blue squares) and ion (red circles) temperature in laser-induced plasma as determined with 2CLS method. The ion temperature was obtained under assumption of two-temperature plasma ($T_e \neq T_i$) and hydrogen atoms following the Boltzmann distribution.

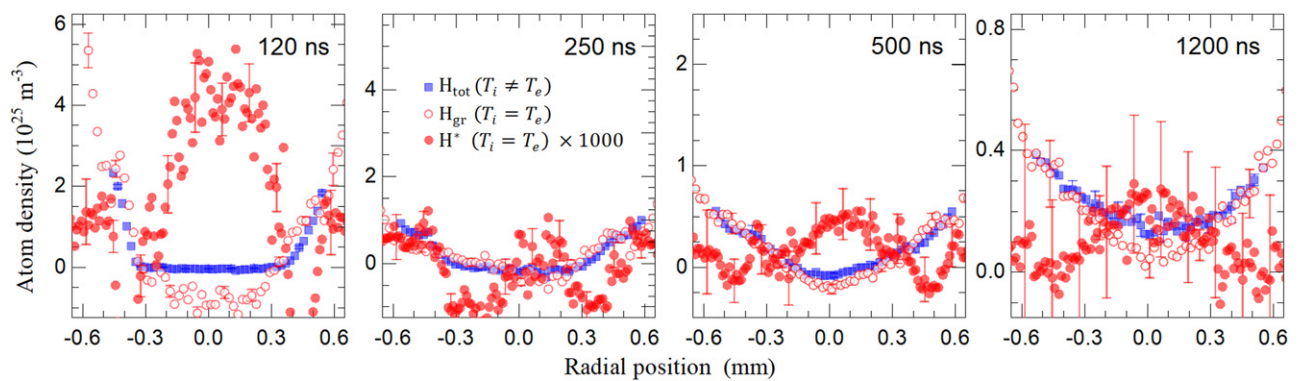


Figure 12. Radial distributions of total (blue squares), ground-state (empty circles) and excited hydrogen atoms (red circles) in laser-induced plasma as determined with 2CLS method. The total density was obtained under assumption of two-temperature plasma and hydrogen atoms following the Boltzmann distribution while the other two assuming the isothermal plasma in partial LTE, i.e. excited atoms follow the Boltzmann distribution with excitation temperature equal to the electron temperature.

$4 \times 10^{22} \text{ m}^{-3}$ to about $2 \times 10^{21} \text{ m}^{-3}$ at delays of 120 ns and 1200 ns, respectively with the detection limit set at about $5 \times 10^{20} \text{ m}^{-3}$.

In some regions of the plasma, the nonphysical (negative) densities of hydrogen atoms are evaluated. It is definitely caused by weak signal-to-noise ratio of measured LS signals and the uncertainty of the cross-sections used. However, this is most likely the result of not entirely satisfied assumptions about the thermodynamic equilibrium of the plasma, but also of the omission of some other processes that might contribute to the scattering signals.

5. Summary and conclusions

In this study, we propose two-color laser scattering (2CLS) as a method to measure electron and neutral densities and electron and ion temperatures in hydrogen plasma. These plasma parameters are determined from TS and RS signals contributing to the overall LS, which are resolved by using two probe lasers (the second and third harmonics of the Nd:YAG laser) of significantly different wavelengths and by

leveraging different wavelength dependencies of the respective cross-sections.

The feasibility of the 2CLS method was studied for various hydrogen plasma conditions, the composition of which was simulated using the NASA CEA equilibrium code, while the cross-sections for RS by ground-state and excited hydrogen atoms were calculated using the Penney approach.

As a proof of principle, 2CLS was applied to investigate the laser-induced hydrogen plasma at 1300 mbar. Temporally and spatially resolved plasma parameters were measured at different moments of plasma evolution. For example, n_e was found to drop from $4.3 \times 10^{23} \text{ m}^{-3}$ to $1.2 \times 10^{22} \text{ m}^{-3}$ in the range of 120 ns to 1200 ns after the pump laser pulse. In the same time interval, n_{H^*} varies from $4 \times 10^{22} \text{ m}^{-3}$ to $2 \times 10^{21} \text{ m}^{-3}$. Moreover, while for most of the plasma conditions investigated, the electron and ion temperatures are consistent with each other, for the shortest delay (120 ns) T_i is about twice as high as T_e . This effect can be explained by the rapid cooling of electrons in the process of radiative emission.

We hope that the results of this work will prove useful in the study of hydrogen plasma such as that found in fusion devices.

However, regardless of the type of plasma, the accuracy of the results obtained by the 2CLS method largely depends on the accuracy of the available cross-sections, including the Rayleigh scattering by excited hydrogen atoms, which currently calls for improved calculations.

Acknowledgments

FS wishes to acknowledge the partial support of this work by the National Science Center Grant No. 2019/33/N/ST2/02823 and by the Polish Ministry of Science and Higher Education Grant No. 2020-N17/MNW/000010.

Data availability statement

The data that support the findings of this study are available upon reasonable request from the authors.

ORCID iDs

Franciszek Sobczuk  <https://orcid.org/0000-0001-9192-8071>

Krzysztof Dzierżęga  <https://orcid.org/0000-0002-6708-7775>

Bartłomiej Pokrzywka  <https://orcid.org/0000-0002-6994-6932>

Evgeny Stambulchik  <https://orcid.org/0000-0002-7100-8793>

References

- [1] Hutchinson I H 2002 *Principles of Plasma Diagnostics* (Cambridge: Cambridge University Press)
- [2] Froula D H, Glenzer S H, Luhmann N C and Sheffield J 2011 *Plasma Scattering of Electromagnetic Radiation: Theory and Measurement Techniques* (New York: Academic)
- [3] Huang M and Hieftje G M 1985 *Spectrochim. Acta B* **40** 1387
- [4] Jauernik P, Kempkens H and Uhlenbusch J 1987 *Plasma Phys. Control. Fusion* **29** 1615
- [5] Bowden M D et al 1993 *J. Appl. Phys.* **73** 2732
- [6] de Regt J M, Engeln R A H, de Groote F P J, van der Mullen J A M and Schram D C 1995 *Rev. Sci. Instrum.* **66** 3228
- [7] Wesseling H J and Kronast B 1996 *J. Phys. D: Appl. Phys.* **29** 1035
- [8] Kempkens H and Uhlenbusch J 2000 *Plasma Sources Sci. Technol.* **9** 492
- [9] Muraoka K, Uchino K, Yamagata Y, Noguchi Y, Mansour M, Suanpoot P, Narishige S and Noguchi M 2002 *Plasma Sources Sci. Technol.* **11** A143
- [10] Fünfer H K E, Kronast B and Kunze H-J 1963 *Phys. Lett.* **5** 125
- [11] Kunze H J, Fünfer E, Kronast W H K B and Kegel W H 1964 *Phys. Lett.* **11** 42
- [12] Wrubel T, Glenzer S, Büscher S and Kunze H J 1996 *J. Atmos. Terr. Phys.* **58** 1077
- [13] Wrubel T, Büscher S and Kunze H J 2000 *Plasma Phys. Control. Fusion* **42** 519
- [14] DeSILVA A W, Evans D E and Forrest J M 1964 *Nature* **203** 1321
- [15] Döbele H F and Hirsch K 1975 *Phys. Lett. A* **54** 267
- [16] van de Sanden M C M, Janssen G M, de Regt J M, Schram D C, van der Mullen J A M and van der Sijde B 1992 *Rev. Sci. Instrum.* **63** 3369
- [17] Murphy A and Farmer A 1992 *J. Phys. D: Appl. Phys.* **25** 634
- [18] Snyder S C, Reynolds L D, Lassahn G D, Fincke J R and KearneyShaw R J 1993 *Phys. Rev. E* **47** 1996
- [19] Snyder S C, Crawford D M and Fincke J R 2000 *Phys. Rev. E* **61** 1920
- [20] Gregori G, Kortshagen U, Heberlein J and Pfender E 2002 *Phys. Rev. E* **65** 046411
- [21] Dzierżęga K, Zawadzki W, Pokrzywka B and Pellerin S 2006 *Phys. Rev. E* **74** 026404
- [22] van Gessel A F H, Carbone E A D, Bruggeman P J and van der Mullen J J A M 2012 *Plasma Sources Sci. Technol.* **21** 015003
- [23] Hübner S, Sousa J S, van der Mullen J and Graham W G 2015 *Plasma Sources Sci. Technol.* **24** 054005
- [24] Banasek J T, Rocco S V R, Potter W M, Lavine E S, Kusse B R and Hammer D A 2020 *Phys. Plasmas* **27** 062708
- [25] Forrest M J, Carolan P G and Peacock N J 1978 *Nature* **271** 718
- [26] Glenzer S H et al 1999 *Phys. Rev. Lett.* **82** 97
- [27] Yamada I, Narihara K, Funaba H, Minami T, Hayashi H and Kohmoto T 2010 *Fusion Sci. Technol.* **58** 345
- [28] Follet R K, Delettrez J A, Edgell D H, Henchen R J, Katz J, Myatt J F and Froula D H 2016 *Rev. Sci. Instrum.* **87** 11E401
- [29] Froula D H, Ross J S, Divol L and Glenzer S H 2006 *Rev. Sci. Instrum.* **77** 10E522
- [30] Pokrzywka B, Mendys A, Dzierżęga K, Grabiec M and Pellerin S 2012 *Spectrochim. Acta B* **T161** 014050
- [31] Dzierżęga K, Mendys A, Pokrzywka B, Zawadzki W and Pellerin S 2013 *Appl. Phys. Lett.* **102** 134108
- [32] Mendys A, Kański M, Farah-Sougueh A, Pellerin S, Pokrzywka B and Dzierżęga K 2014 *Spectrochim. Acta B* **96** 61
- [33] Henchen R J, Sherlock M, Rozmus W, Katz J, Cao D, Palastro J P and Froula D H 2018 *Phys. Rev. Lett.* **121** 125001
- [34] Zhang H, Wu Y, Sun H, Yang F, Rong M and Jiang F 2019 *Spectrochim. Acta B* **157** 6
- [35] Milder A L, Katz J, Boni R, Palastro J P, Sherlock M, Rozmus W and Froula D H 2021 *Phys. Plasmas* **28** 082102
- [36] Pan Y, Tomita K, Uchino K, Sunahara A and Nishihara K 2021 *Appl. Phys. Express* **14** 066001
- [37] Limbach C and Miles R B 2014 *45th AIAA Plasmadynamics and Lasers Conf.* p 1
- [38] Baum D, Hackmann J and Uhlenbusch J 1974 *Plasma Phys.* **17** 79
- [39] Boxman R L 1974 *J. Appl. Phys.* **45** 4835
- [40] Hare J D, MacDonald J, Bland S N, Dranczewski J, Halliday J W D, Lebedev S V, Suttle L G, Tubman E R and Rozmus W 2019 *Plasma Phys. Control. Fusion* **61** 085012
- [41] Gordon S and McBride B J 1996 *Office of Management, Scientific and Technical Information Program* (Cleveland: National Aeronautics and Space Administration)
- [42] Ubachs W, van Duijn E, Vieitez M, Van de Water W, Dam N, ter Meulen J, Meijer A, de Kloe J, Stoffelen A and Aben E 2010 *A Spontaneous Rayleigh-Brillouin Scattering Experiment for the Characterization of Atmospheric LIDAR Backscatter* ESA-TENDER AO/1-467/07/NL/HE
- [43] Penney C 1969 *J. Opt. Soc. Am.* **59** 34
- [44] Gavrilin M 1967 *Phys. Rev.* **163** 147
- [45] Gavrilin M 1979 *Z. Phys. A* **293** 269
- [46] Schulman J M and Musher J I 1968 *J. Chem. Phys.* **49** 4845
- [47] Sobelman I 1992 *Atomic Spectra and Radiative Transitions* (Berlin: Springer)

- [48] McNamara K, Fursa D V and Bray I 2018 *Phys. Rev. A* **98** 043435
- [49] Dzierżęga K, Sobczuk F, Stambulchik E and Pokrzywka B 2021 *Phys. Rev. E* **103** 063207
- [50] Salpeter E 1960 *Phys. Rev.* **120** 1528
- [51] Evans O E and Katzenstein J 1969 *Rep. Prog. Phys.* **32** 207
- [52] Warner K and Hieftje G 2002 *Spectrochim. Acta B* **57** 201
- [53] Dzierżęga K, Mendys A, , and Pellerin S 2014 *Spectrochim. Acta B* **98** 76
- [54] Thalman R, Zarzana K J, Tolbert M A and Volkamer R 2014 *J. Q. Spectrosc. Radiat. Transfer* **147** 171
- [55] Norreys P A et al 2005 *Plasma Phys. Control. Fusion* **47** L49
- [56] Rakowski C E, Ghavamian P and Hughes J P 2003 *Astrophys. J.* **590** 846
- [57] Ghavamian P, Laming J M and Rakowski C E 2007 *Astrophys. J.* **654** L69
- [58] Slavin J A, Smith E J, Sibeck D G, Baker D N, Zwickl R D and Akasofu S I 1985 *J. Geophys. Res.* **90** 10875